HEFAT2010
7th International Conference on Heat Transfer, Fluid Mechanics and Thermodynamics
19-21 July 2010
Antalya, Turkey

Effect of Eccentricity in Horizontal Annulus Using Lbm

Fattahi E.*,.Sedighi K., Farhadi M., Nemati, H.
*Author for correspondence
Department of Mechanical Engineering,
Babol University of Technology, Islamic Republic of Iran,
Babol,
Islamic Republic of Iran,
E-mail: E.Fattahi@stu.nit.ac.ir

ABSTRACT

In this article, the natural convection flow in eccentric annulus is simulated numerically by Lattice Boltzmann Model (LBM) based on double-population approach. A numerical strategy presents for dealing with curved boundaries of second order accuracy for both velocity and temperature fields. The effect of eccentricity at various locations is examined under three scenarios: vertical, horizontal, and diagonal eccentricity arrangements at Ra=10^4 and σ=2. Velocity and temperature distributions as well as Nusselt number are obtained. The results are validated with published results and shown that double-population approach can evaluate the velocity and temperature fields in curved boundaries with a good accuracy in comparison with the previous studies. The results show that the average Nusselt number increases in when the inner cylinder moves downward regardless of the radial position.

INTRODUCTION

The lattice Boltzmann method (LBM) is a powerful numerical technique based on kinetic theory for simulating fluid flows and modeling the physics in fluids [1–4]. In comparison with the conventional CFD methods, the advantages of LBM include simple calculation procedure, simple and efficient implementation for parallel computation, easy and robust handling of complex geometries, and others. Various numerical simulations have been performed using different thermal LB models or Boltzmann-based schemes to investigate the natural convection problems [5–7].

The lattice Boltzmann equation (LBE) is a minimal form of the Boltzmann kinetic equation, and the result is a very elegant and simple evolution equation for a discrete distribution function, or discrete population $f_i(x,t) - f(x,c,t)$, which describes the probability to find a particle at lattice position x at time t, moving with speed c_i .With respect to the more conventional numerical methods commonly used for the study of fluid flow situations, the kinetic nature of LBM (Lattice Boltzmann Method) introduces several advantages, including easy implementation of boundary conditions and fully parallel algorithms. In addition, the convection operator is linear, no

NOMENCLATURE

c_k	[-]	Discrete lattice velocity in direction k
c_s	[-]	Speed of sound in Lattice scale
F_k	[-]	External force in direction of lattice velocity
f_k^{eq}	[-]	Equilibrium distribution
g_y	[ms^{-2}]	Acceleration due to gravity,
k	[w/m.k]	Thermal conductivity
Nu_{av}	[-]	Average Nusselt number
Nu	[-]	Mean Nusselt number
$Nu_{o,i}$	[-]	Local Nusselt number along surfaces
Pr	[-]	Prandtl number
r	[-]	dimensionless radial position ($= R/(R_o - R_i)$)
R	[-]	radial coordinate
rr	[-]	radius ratio, = Ro/Ri
R_i ; R_o	[m]	radii of the inner and outer cylinders, respectively
Ra	[-]	Rayleigh number ($g\beta\Delta TH^3/\alpha\nu$)
T_h	[K]	Hot temperature
T_c	[K]	Cold temperature
T_0	[K]	bulk temperature $T_0=(T_h+T_c)/2$
$u.v$	[m/s]	Horizontal and vertical components of velocity
w	[-]	Weighting factor
Greek symbols		
ε		eccentricity
σ		annulus gap width ratio ($2R_i/(R_o-R_i)$)
φ		tangential direction

Poisson equation for the pressure must be resolved and the translation of the microscopic distribution function into the macroscopic quantities consists of simple arithmetic calculations.

In general, there exist three approaches for incorporating the heat transfer effect into the LBGK method in the literature, one is concerned with multi-speed models [8-10] and the other is passive-scalar approach [11] and the last one is double-population models [12-16]. The first approach can particularly deal with density distribution function and introduce additional

discrete velocities to obtain macroscopic energy equations and equilibrium distribution which usually include higher order velocity terms. In the second approach, a separate distribution function which is independent of the density distribution function proposed [11] and in the third approach, an independent LBGK equation temperature is introduced in addition to the original distribution function of density.

The coupling between the two LBGK equations can be implemented in different ways [17-22]. This type of model is usually adopted in practical application, because the multi-speed approach suffers from severally numerical instability [12] and limits in a rather narrow temperature range and in the passive-scalar approach, the viscous heat dissipation and compression work done by the pressure can not be taken into account [12]. Therefore, in the present study, a type of double-population model is integrated in the numerical scheme.

The geometry of the horizontal annuli is commonly found in solar collector-receiver, under ground electric transmission cables, vapor condenser for water distillation and food process. Numerical simulation of natural convection in concentric and eccentric circular cylinder has been studied rigorously in the literatures [23-25]. Kuhen and Goldsein [26-28] conducted an experimental and theoretical study of natural convection in concentric and eccentric horizontal cylindrical annuli. Their experimental data is commonly used to validate most of the recent numerical studies. Ho and Lin [29] presented heatlines for steady laminar two-dimensional natural convection in concentric and eccentric horizontal cylindrical annuli with mixed boundary conditions. Glakpe et al. [30] presented numerical solutions for steady laminar two-dimensional natural convection in annuli between concentric and vertically eccentric horizontal circular cylinders. Guj and Stella [31] presented numerical and experimental buoyancy driven flow in horizontal annulus. They studied the effect of the horizontal eccentricity and found that the average Nusselt number is nearly independent of the horizontal eccentricity.

In the present study, an extrapolation Method based on Gou et al. [32] was used to simulate natural convection in horizontal eccentric annulus. The method combined with the velocity boundary presented in Mei et al. [33] can indeed achieve second-order accuracy for both velocity and temperature on the curved wall. The effect of vertical, horizontal and diagonal eccentricity is examined in this study and the numerical results are compared with previous experimented and numerical data.

LATTICE BOLTZMANN METHOD

The Lattice Boltzmann Method (LBM) divide time and space into steps to form a lattice and discretize the fluid as particles, which are positioned at certain points in space, called lattice sites or cells. These fluid particles are only allowed to move in certain and fixed directions, which are derived by a discretization of velocity space. In the LBM, the particle represented by distribution function .This distribution function is calculated by solving the Lattice Boltzmann equation (without external force) equation (1), which is a special discretization of the kinetic Boltzmann equation. The macroscopic quantities of the simulated fluid can then be derived by calculating the hydrodynamic moments of the distribution function. In contrast to the second-order PDEs in the NS approach, the LBM uses only first order PDEs.

$$\frac{\partial f}{\partial t} + c.\nabla f = -\frac{1}{\tau}(f - f^{eq}) \tag{1}$$

Where c is the particle velocity vector, f^{eq} is the equilibrium distribution function and τ is the relaxation time due to collision [20] and depending on the fluid viscosity.

By a discretization in velocity space, a finite set of velocity vectors is derived, which have to conserve mass, momentum and energy of the fluid particles (conservation laws). Equation (2) shows the discretized formulation of equation (1). f_α denotes the corresponding distribution function in direction α, which is associated with the discrete velocity c_α in direction α and f_α^{eq} is the corresponding equilibrium distribution function [20]:

$$\frac{\partial f_\alpha}{\partial t} + c_\alpha.\nabla f_\alpha = -\frac{1}{\tau}\left(f_\alpha - f_\alpha^{eq}\right) \tag{2}$$

In this work the velocity space discretization in the two dimensional case is the D2Q9 model [20]. In this model, the velocity space is discretized in 9 distribution functions, which is the most popular model for the 2D case (Figure 1).

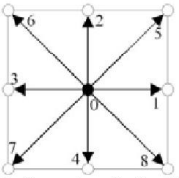

Figure 1 Discrete velocity vectors for the D2Q9 model for 2D LBM

In the following, $\mathbf{e}_\alpha$ will denote the discrete velocity set, where α is between 0 and 8.

$$\mathbf{e}_\alpha = \begin{cases} (0,0) & \alpha = 0 \\ (\cos[(\alpha-1)\pi/4], \sin[(\alpha-1)\pi/4])c & \alpha = 1,2,3,4 \\ \sqrt{2}(\cos[(\alpha-1)\pi/4], \sin[(\alpha-1)\pi/4])c & \alpha = 5,6,7,8 \end{cases} \tag{3}$$

Where $c - \Delta x / \Delta t$, Δx and Δt are the lattice cell size and the lattice time step size, respectively.

For the D2Q9 model, the equilibrium distribution function of equation (2) is expressed as:

$$f_\alpha^{eq} = w_\alpha\left(1 + \frac{3}{c^2}\mathbf{e}_\alpha.\mathbf{u} + \frac{9}{2c^4}(\mathbf{e}_\alpha.\mathbf{u})^2 - \frac{3}{2c^2}\mathbf{u}.\mathbf{u}\right) \tag{4}$$

Where:

$$w_\alpha = \begin{cases} 4/9 & \alpha = 0 \\ 1/9 & \alpha = 1,2,3,4 \\ 1/36 & \alpha = 5,6,7,8 \end{cases} \tag{5}$$

w_α is the equilibrium distribution weight for direction α.

The fluid density ρ can be evaluated with equation (6), whereas the velocity $\mathbf{u}$ is contained in the momentum fluxes of equation (7):

$$\rho = \sum_\alpha f_\alpha \tag{6}$$

$$\rho\mathbf{u} = \sum_\alpha \mathbf{e}_\alpha f_\alpha \tag{7}$$

Equation (2) is called the discrete velocity model (DVM). This equation can be solved by the standard numerical approaches,

for example Finite Difference Method. The LBM approach uses this method for discretization of equation (2):

$$f_\alpha(\mathbf{x}+e_\alpha\Delta t,t+\Delta t)-f_\alpha(\mathbf{x},t)=-\frac{1}{\tau_m}\left[f_\alpha(\mathbf{x},t)-f_\alpha^{eq}(\mathbf{x},t)\right]+\Delta t\, e_\alpha.F_k \tag{8}$$

Where τ_m denotes the lattice relaxation time $(\tau_m = 3\nu + 1/2)$.

For incompressible flow the lattice Boltzmann equation of temperature field can be given by:

$$g_\alpha(\mathbf{x}+e_\alpha\Delta t,t+\Delta t)-g_\alpha(\mathbf{x},t)=-\frac{1}{\tau_T}\left[g_\alpha(\mathbf{x},t)-g_\alpha^{eq}(\mathbf{x},t)\right] \tag{9}$$

Where g_α is temperature distribution function in the α direction, τ_T is the relaxation time $(\tau_T = 3\sigma + 1/2)$ and g_α^{eq} is the corresponding equilibrium distribution function and can be expressed as [21, 22]:

$$g_\alpha^{eq}=w_\alpha T(1+\frac{3}{c^2}\mathbf{e}_\alpha.\mathbf{u}) \tag{10}$$

Where T is the fluid temperature and can be evaluated from:

$$T=\sum_\alpha g_\alpha \tag{11}$$

Finally, equation (8) and equation (10) is usually solved in two steps:

Collision step

$$\tilde{f}_\alpha(\mathbf{x},t+\Delta t)=-\frac{1}{\tau_m}\left[f_\alpha(\mathbf{x},t)-f_\alpha^{eq}(\mathbf{x},t)\right]-f_\alpha(\mathbf{x},t) \tag{12}$$

Streaming step

$$f_\alpha(\mathbf{x}+e_\alpha\Delta t,t+\Delta t)=\tilde{f}_\alpha(\mathbf{x},t+\Delta t) \tag{13}$$

Where $\tilde{f}_\alpha,\tilde{g}_\alpha$ denotes the post-collision distribution function. Equation (12) is the so called collision step. This step models various fluid particle interactions like collisions and calculates new distribution functions according to the distribution functions of the last time step and the equilibrium distribution functions, which are calculated with equation (4) and equation (10). The second step is called stream step. In this step, fluid particles are streamed from one cell to a neighbouring cell according to the velocity and temperature of the fluid particles in this cell.

Curve boundary treatment

Consider Figure 2 is a part of an arbitrary curved wall geometry, where the black small circles on the boundary $\mathbf{x}_w$, the open circles represent the boundary nodes in the fluid region $\mathbf{x}_f$ and the grey circles indicate those in the solid region $\mathbf{x}_b$. In the boundary condition $\tilde{f}(\mathbf{x}_b,t),\tilde{g}(\mathbf{x}_b,t)$ are needed to perform the streaming steps on fluid nodes $\mathbf{x}_f$.

The fraction of an intersected link in the fluid region Δ is defined by:

$$\Delta=\frac{\|\mathbf{x}_f-\mathbf{x}_w\|}{\|\mathbf{x}_f-\mathbf{x}_b\|} \tag{14}$$

To calculate the distribution function in the solid region $\tilde{f}_{\bar{\alpha}}(\mathbf{x}_b,t)$ based upon the boundary nodes in the fluid region, the bounce-back boundary conditions combined with interpolations including a one-half grid spacing correction at the boundaries [15].

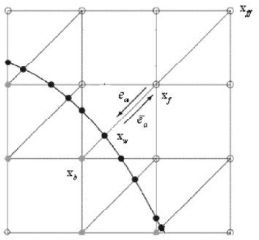

Figure 2 lattices in curved wall boundary

Then the Chapman–Enskog expansion for the post-collision distribution function on the equation (12a) is conducted as:

$$\tilde{f}_{\bar{\alpha}}(\mathbf{x}_b,t+\Delta t)=(1-\lambda)\tilde{f}_\alpha(\mathbf{x}_f,t+\Delta t)+\lambda f_\alpha^*(\mathbf{x}_b,t+\Delta t) -2\frac{3}{c^2}w_\alpha\rho(\mathbf{x}_f,t+\Delta t)\mathbf{e}_\alpha.\mathbf{u}_w \tag{15}$$

Where

$$f_\alpha^*(\mathbf{x}_b,t+\Delta t)=f_\alpha^{eq}(\mathbf{x}_f,t+\Delta t)+ \frac{3}{c^2}w_\alpha\rho(\mathbf{x}_f,t+\Delta t)\mathbf{e}_\alpha.(\mathbf{u}_{bf}-\mathbf{u}_f) \tag{16}$$

$$\mathbf{u}_{bf}=\mathbf{u}_{ff},\qquad \lambda=\frac{2\Delta-1}{\tau_m-2},\quad if\ \ 0<\Delta\le\frac{1}{2} \tag{17a}$$

$$\mathbf{u}_{bf}=(1-\frac{3}{2\Delta})\mathbf{u}_f+\frac{3}{2\Delta}\mathbf{u}_w,\quad \lambda=\frac{2\Delta-1}{\tau_m+1/2},\ if\ \ \frac{1}{2}<\Delta\le 1 \tag{17b}$$

$\mathbf{u}_w$ denotes the velocity of solid wall, $\mathbf{u}_{bf}$ is the imaginary velocity for interpolations and $\mathbf{e}_{\bar{\alpha}}\equiv-\mathbf{e}_\alpha$.

For temperature field in curved boundary this study use the method is based on the method reported in [15]. Distribution function for temperature divided two parts, equilibrium and non equilibrium:

$$g_{\bar{\alpha}}(\mathbf{x}_b,t)=g_{\bar{\alpha}}^{eq}(\mathbf{x}_b,t)+g_{\bar{\alpha}}^{neq}(\mathbf{x}_b,t) \tag{18}$$

By substituting equation (18) into equation (12) we have:

Equilibrium and non equilibrium parts of equation (19) are define as:

$$g_{\bar{\alpha}}^{eq}(\mathbf{x}_b,t)=w_{\bar{\alpha}}T^*(1+\frac{3}{c^2}\mathbf{e}_{\bar{\alpha}}.\mathbf{u}_b^*) \tag{20}$$

$$g_{\bar{\alpha}}^{neq}(\mathbf{x}_b,t)=g_{\bar{\alpha}}^{neq}(\mathbf{x}_f,t)\quad if\quad \Delta\ge 0.75 \tag{21a}$$

$$g_\alpha^{neq}(\mathbf{x}_b,t)=\Delta g_\alpha^{neq}(\mathbf{x}_f,t)+(1-\Delta)g_\alpha^{neq}(\mathbf{x}_{ff},t)\quad if\quad \Delta<0.75 \tag{21b}$$

RESULT AND DESCUSION

The present investigation considers two infinite horizontal circular cylinder of inner and outer radius, R_i and R_o, respectively. A radial temperature gradient (ΔT) is applied with subjecting the walls of the inner cylinder to a higher temperature (T_h) than its outer cylinder counterpart (T_c).

To validate the numerical simulation, local and equivalent thermal conductivity is obtained at for a natural convection in eccentric horizontal annulus. Results have been compared with the study of Kuehn and Goldstein [26]. An equivalent thermal conductivity, K_{eq} is used to compare the accuracy of the present computations. The average equivalent heat conductivity defined for inner and outer cylinder by:

$$\overline{K}_{eqi} = -\frac{\ln(rr)}{\pi(rr-1)}\int_0^{\pi}\frac{\partial T}{\partial r}d\varphi$$

$$\overline{K}_{eqo} = -\frac{rr.\ln(rr)}{\pi(rr-1)}\int_0^{\pi}\frac{\partial T}{\partial r}d\varphi$$

This parameter is defined as the actual heat flux divided by the heat flux that would be occurred by pure conduction in the absence of fluid motion. The computed average equivalent heat conductivity for eccentric annulus at Pr=0.71 and rr=2.6 are compared with the previous study [27]. Results of local equivalent thermal conductivity are shown in Fig. 5 and represent good agreement between the present computations and experiments of Kuhen and Goldstein [27]. In particular, the present local equivalent thermal conductivity results are well within ±3% of the benchmark data by Kuehn and Goldstein.

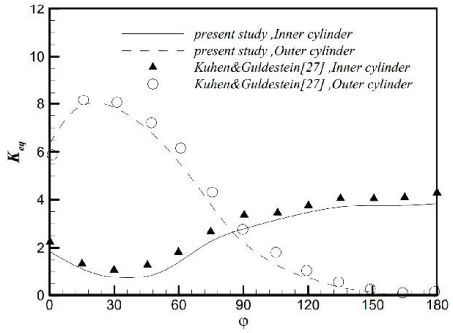

Figure 5. Comparison of Equvalent thermal conducivity on inner and outer cylinder with experimental deta [27], for ε=(3/4,0) at Ra=5×10^4 and rr=2.6.

For further validation of the Numerical procedure isotherms and streamlines pattern for different eccentric annulus are compared with the experimental results obtained by Guj & Stella [31]. a vertical eccentric location ε=(1/4,-π/2)) is examined at σ=1.47 and found to establish a good agreement between them, which is shown in Figure 6.

The effect of eccentricity at various locations is examined under three scenarios: vertical, horizontal, and diagonal eccentricity arrangements at Ra=10^4 and σ=2. The effect of vertical eccentricity on the flow and thermal fields is shown in Figure 7(a)-(d), with streamlines (left) and the isotherms (right). Two large recirculation cells appear within the annular cylinders. While the inner cylinder moves upward, the narrow space above the inner cylinder inhibits the circulation of the hot moving fluid as shown in Figure 7(a). As a result, Conduction heat transfer becomes dominant. When the fluid returns along the outer cylinder, the flow cools and approaches a region of relatively stagnant fluid where convection is weak. An increase in the cell strength occurs when the inner cylinder moves downward, so, the convection heat transfer becomes dominant (Fig 7(c) and (d)). For better discussion present investigation is concluded by exploring the effect of the vertical eccentricity on the local Nu number outcome.

Figure 8(a) and (b) show that the local Nusselt number for ε=(3/4,0) starts from a local maximum (top of the annulus) which is due to the domination of the conduction heat transfer between the inner and the outer cylinders.

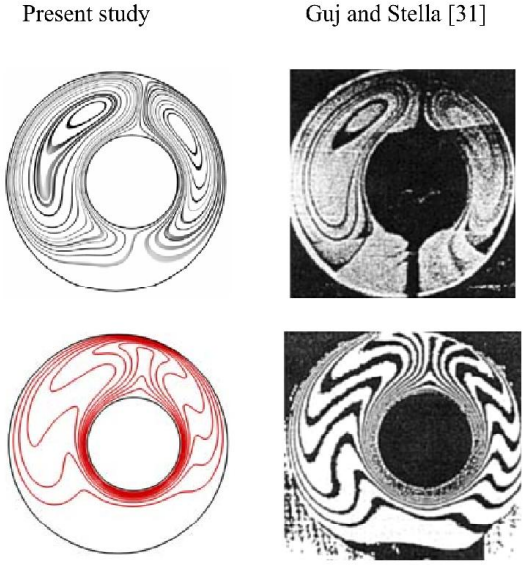

Figure 6. Comparison of streamlines (top) and isotherms (bottom) for ε=(1/4,-π/2), Ra=4.59×10^4 between the present work and experimental study of Guj and Stella [31] using σ=1.47.

The effect of convection becomes more inhibited in the region between the inner and outer cylinders for ε= (3/4, 0); this is understandable since the upper region is now inadequate to permit rapid acceleration of fluid motion around the inner cylinder.

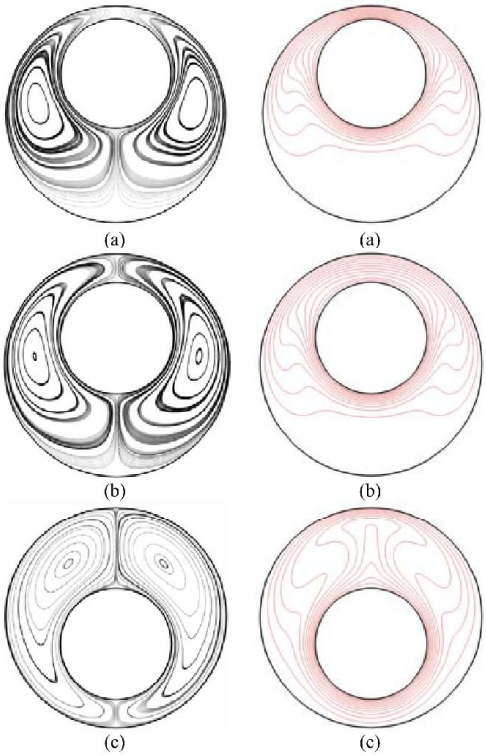

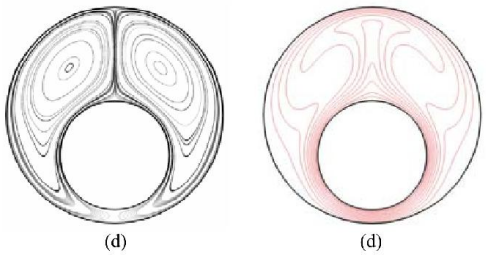

Figure 7. Streamline (left) and isotherm (right) under different vertical eccentricity locations for σ=2 at Ra=104 using: (a)ε=(3/4,0); (b)ε=(1/2,0) ; (c)ε=(1/2,π) ; (d)ε=(3/4,π)

When the inner cylinder move downward, Nu number starts from local minimum and then increases smoothly.

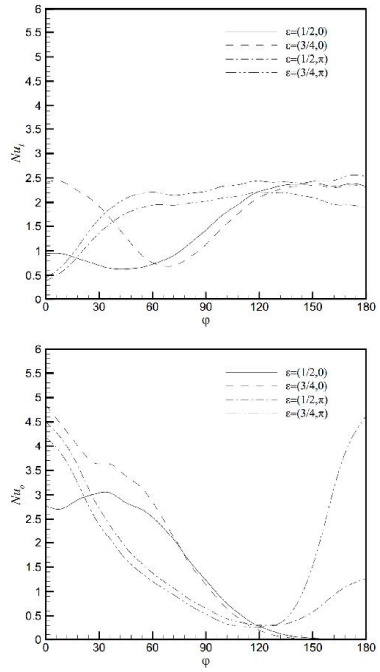

Figure 8. Local Nusselt number variation at the: (a) inner and (b) outer cylinder different vertical eccentricity locations for σ=2 at Ra=10^4

When the flow approaches the top of the inner cylinder, buoyancy causes the fluid to arise. Thus, the boundary layer decelerates at the top of the inner cylinder and separates from the surface and consequently, convection becomes dominant. As the flow travels around the inner cylinder; the conduction heat transfer dominates between the two cylinders at the bottom of the inner cylinder.

The effect of horizontal eccentricity locations is shown in Figure 9. when the inner cylinder moves to the right (or left) of the outer cylinder, two rotating cell form in the enclosure, the main and the larger rotating cell on the left, the small and secondary cell at the right. It's due to flow inhibition between two cylinder surfaces at the right; convection heat transfer decreases and conduction increases. This effect can be seen in local Nusselt distribution. The effect of convection becomes

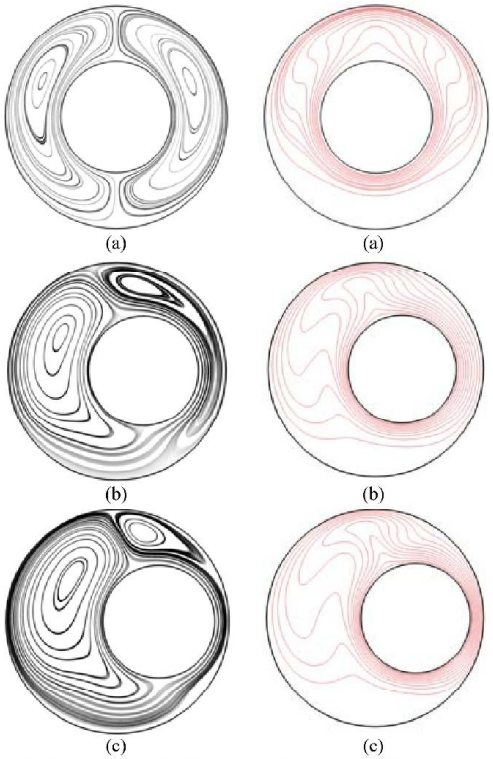

Figure 9. Streamline (left) and isotherm (right) patterns under different horizontal eccentricity locations for σ=2 at Ra=10^4 using: (a)ε=(0,0); (b)ε=(1/2,-π/2) ; (c)ε=(3/4,-π/2)

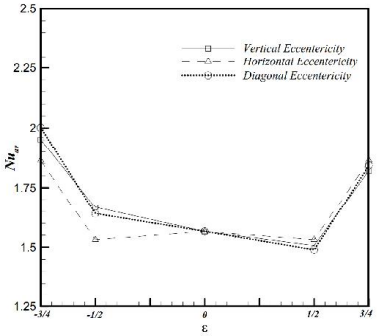

Figure 13. Average Nusselt number versus eccentricity

more inhibited in the region between cylinder surfaces for ε= (3/4, -π/2). Similar phenomena can be observed for the inner cylinder moving aligned. local Nu values tend to peak when the inner cylinder moving closer to the outer cylinder (ε=(3/4,-π/4) and ε=(3/4,-3π/4)).

Figure 13 shows the effect of eccentricity positioning on average Nu number. The results show that the eccentricity significantly influences the heat transfer. It can be seen that heat transfer augmentation is higher for a dimensionless radial position of r=3/4, which is the case when the inner cylinder is placed away from the center and closer to the outer cylinder. When the inner cylinder, moves downward closer to the outer

cylinder, i.e r=3/4, the Nusselt number increases approximately 25% in comparison with the concentric configuration. Furthermore, Figure 13 shows an increase in the average Nusselt number when the inner cylinder moves downward regardless of the radial position.

CONCULSION

Natural convection flow in eccentric annulus was simulated numerically at $Ra=10^4$ and $\sigma=2$. The Lattice Boltzmann method based on double-population was used for dealing with curved boundaries for flow and thermal fields. The problem was solved and some conclusions were summarized as follows:

a. Lattice Boltzmann method based on double-population is a powerful approach for simulating natural convection in the geometry that include curved boundaries. This method can simulate the velocity and temperature fields with second order accuracy.
b. Heat transfer augmentation is higher for a dimensionless radial position of r=3/4, which is the case when the inner cylinder is placed away from the center and closer to the outer cylinder.
c. An increase in the average Nusselt number occurred when the inner cylinder moves downward regardless of the radial position.
d. Computational results support data previously published in the literature.

REFERENCES

[1] Qian Y.H., d'Humieres D., Lallemand P ., Lattice BGK models for Navier–Stokes equation, Europhys. Lett. 17 (6) (1992) 479–484.
[2] Chen S., Doolen G.D., Lattice Boltzmann method for fluid flows, Annu. Rev. Fluid Mech. 30 (1998) 329–364.
[3] Yu D., Mei R., Luo L. S., Shyy W., Viscous flow computations with the method of lattice Boltzmann equation, Progr. Aerospace Sci. 39 (2003) 329–367.
[4] Succi S., The Lattice Boltzmann Equation for Fluid Dynamics and Beyond, Clarendon Press, Oxford, 2001.
[5] Kao P. H., Yang R. J., Simulating oscillatory flows in Rayleigh–Benard convection using the lattice Boltzmann method, Int. J. Heat Mass Transfer 50 (2007) 3315–3328.
[6] Dixit H. N., Babu V., Simulations of high Rayleigh number natural convection in a square cavity using the lattice Boltzmann method, Int. J. Heat Mass Transfer 49 (2006) 727–739.
[7] Zhou Y., Zhang R., Staroselsky I., Chen H., Numerical simulation of laminar and turbulent buoyancy-driven flows using a lattice Boltzmann based algorithm, Int. J. Heat Mass Transfer 47 (2004) 4869–4879.
[8] Alexander F.J., Chen S., Sterling J.D., Lattice Boltzmann thermo hydrodynamics, Phys. Rev. E 47 (4) (1993) R2249–R2252.
[9] Teixeira C., Chen H., Freed D. M., Multi-speed thermal lattice Boltzmann method stabilization via equilibrium under-relaxation, Comput. Phys. Commun. 129 (1/3) (2000) 207–226.
[10] Watari M., Tsutahara M., Possibility of constructing a multispeed Bhatnagar-Gross-Krook thermal model of the lattice Boltzmann method, Phys. Rev. E 70 (2004) 1/016703–9/016703.
[11] X. Shan, phys. Rev. E 55, 2780(1997)
[12] He X., Chen S., Doolen G.D., A novel thermal model for the lattice Boltzmann method in incompressible limit, J. Comput. Phys. 146 (1998) 282–300.
[13] Shan X., Simulation of Rayleigh–Benard convection using a lattice Boltzmann method, Phys. Rev. E 5 5 (1997) 2780–2788.
[14] Peng Y., Shu C., Chew Y.T., Simplified thermal lattice Boltzmann model for incompressible thermal flows, Phys. Rev. E 6 8 (2003) 026701.
[15] Guo Z.L., Shi B.C., Zheng Ch., A coupled lattice BGK model for the Boussinesq equations, Int. J. Numer. Methods Fluids 39 (4) (2002) 325–342.
[16] Shi Y., Zhao T.S., Guo Z.L., Thermal lattice Bhatnagar–Gross–Krook model for flows with viscous heat dissipation in the incompressible limit, Phys. Rev. E 70 (2004) 1–10.
[17] Palmer BJ., Rector DR., Lattice Boltzmann algorithm for simulating thermal flow in compressible fluids. J Comput Phys 161(2000)1–20.
[18] Guo ZL., Zhao TS., A lattice Boltzmann model for convection heat transfer in porous media. Numer. Heat Transfer B Fund. 47 (2005) 157–177
[19] Guo ZL., Zhao TS., Lattice Boltzmann simulation of natural convection with temperature-dependent viscosity in a porous cavity. Prog Comput Fluid Des 5(1/2)(2005) 110–7.
[20] Van Der Sman RGM. Lattice Boltzmann scheme for natural convection in porous media. Int J Mod Phys C 8 (1997)879–88.
[21] Peng Y, Chew YT, Shu C. Numerical simulation of natural convection in a concentric annulus between a square outer cylinder and a circular inner cylinder using the Taylor series expansion and least square based lattice Boltzmann method. Phys Rev E 67 (2003).
[22] Peng Y, Shu C, Chew YT. A 3D incompressible thermal lattice Boltzmann model and its application to simulate natural convection in a cubic cavity. J Comput Phys 193 (2003)260–74.
[23] Glakpe E. K., Watkins C. B., and Cannon J. N., Constant Heat-Flux Solutions for Natural Convection between Concentric and Eccentric Horizontal Cylinders, Numer. Heat Transfer, vol. 10(1986)279–295,
[24] Lee T. S., Hu G. S., and Shu C., Application of GDQ Method for the Study of Natural Convection in Horizontal Eccentric Annuli, Numer. Heat Transfer, vol. 41(2002) 803–815,
[25] F. Moukalled and S. Acharya, Laminar Natural Convection Heat Transfer in an Eccentric Rhombic Annulus, Numer. Heat Transfer, vol. 26(1994)551–568.
[26] Kuehn T, Goldstein R. An experimental and theoretical study of natural convection in the annulus between horizontal concentric cylinders. J Fluid Mech 74 (1976)695–719.
[27] Kuehn T, Goldstein R. An experimental study of natural convection heat transfer in concentric and eccentric horizontal cylindrical annuli. J Heat Transfer 100 (1978)635–40.
[28] Kuehn T, Goldstein R. A parametric study of Prandtl number and diameter ratio effects on natural convection heat transfer in horizontal cylindrical annuli. J Heat Transfer 102 (1978)768–770.
[29]. E. K. Glapke, C. B. Watkins, and J. N. Cannon, Constant Heat Flux Solutions for Natural Convection between Concentric and Eccentric Horizontal Cylinders, Numer. Heat Transfer, VO~10. , 279-295, 1986.
[30] C.J. Ho, Y.H. Lin, A numerical study of natural convection in concentric and eccentric horizontal cylindrical annuli with mixed boundary conditions, Int. J. Heat Fluid Flow 10 (1989) 40–47.
[31] Guj G, Stella F. Natural convection in horizontal eccentric annuli: numerical study. Numer Heat Transfer Part A 1995;27:89–105.
[32] Guo Z.L., Zheng Ch., Shi B.C., An extrapolation method for boundary conditions in lattice Boltzmann method, Phys. Fluids 14 (6) (2002) 2007–2010.
[33] Mei R., Yu D., Shyy W., Luo L.Sh., Force evaluation in the lattice Boltzmann method involving curved geometry, Phys. Rev. E 65 (2002) 1–14.